Reconstructing ocean conditions and latitudinal migration of oceanic fronts offshore Tasmania during the mid-Pliocene using high-resolution dinoflagellate cyst assemblages from IODP Site 1168A.

27 pages

9 figures, 1 table

submitted as

Master Thesis

at the

Faculteit Geowetenschappen

Universiteit Utrecht

by

Kim Leonie Toebrock

Supervisors:

Dr. Peter Bijl

Dr. Francesca Sangiorgi

Suning Hou MSc

1 Abstract

The mid-Pliocene was characterised by a warm climate with similar CO_2 concentrations to today but higher sea levels which suggests a contribution from the Antarctic Ice Sheet. This warm climate was disrupted by the transient M2 glaciation at 3.3 Ma before returning to warmer conditions during the mPWP (3.264 Ma). This glaciation has generally been seen as a Northern Hemisphere glaciation, but recent studies have shown evidence that the Antarctic Ice Sheet must have been more affected by warming and cooling during the Pliocene. Uncertainties remain on how large that glaciation was and what the ocean conditions around Antarctica were before 3.3 Ma. The Southern Ocean is strongly latitudinally banded, which is indicated by the 3 Southern Ocean fronts. Glacial-interglacial climate variability strongly moves those latitudinal bands north and south. Changes in the configuration of the Antarctic Ice Sheet impact the latitudinal location of these fronts, as they are linked through sea ice season. To better understand how ocean conditions in the Southern Ocean changed in association with the mPWP and the M2 glaciation, we use dinoflagellate cyst assemblages from Site 1168, on the western margin of Tasmania, to reconstruct latitudinal Subtropical Front movement. We found a significant dinocyst assemblage change across the M2 glaciation. Before and after the M2, the dinocyst assemblage was dominated by *O. centrocarpum* which is indicative of a position north of the STF, while during the M2, there was a transient *N. labyrinthus* assemblage dominance which is indicative for a position south of the STF. Such an assemblage change indicates a migration of the STF, of around 3-4° latitude. Thus, we infer that the Antarctic Ice Sheet must have been more dynamic in the mid-Pliocene than previously assumed. Based on the observed latitudinal migration of the Subtropical Front, the Antarctic ice sheet must have extended and decreased across the Pliocene. In addition, by comparing with biomarker-based SST, we found an offset between changing SST and the maximum response of the dinocyst assemblage which can be linked to influxes of freshwater during the deglaciation of the M2 affecting the maximum relative abundance of certain species. Overall, our data proved that the Antarctic ice sheet was more sensitive to the variable Pliocene climate.

Table of Content

2 Introduction

Geological records of past climates provide the opportunity to understand how Earth`s climate will behave in the future given the current unequivocal warming (Haywood et al., 2016). For this, the evolution of the Southern Ocean (SO) is particularly important, as it plays a crucial role in (1) distributing heat, (2) deep ocean circulation, (3) stability of the Antarctic ice sheet, and (4) carbon exchange between the atmosphere to the ocean (Marshall & Speer, 2012; Lenton & Matear 2007).

The Antarctic circumpolar current (ACC) is the major current system in the SO which connects all ocean basins and flows clockwise around Antarctica (Ballegeer et al., 2012; Graham, et al., 2013). Its boundaries are based on density, salinity and temperature (Graham, 2014; Chapman et al., 2020; Graham & De Boer, 2013). The ACC consists of 3 fronts. The subtropical front (STF) represents the northern limit of the ACC and the Polar Front to the southern. In between these, the Subantarctic Front is situated (Gille et al., 2016; Orsi et al., 1995; Ballegeer et al., 2012). These fronts divide 3 different zones, from north to south: The sub-Antarctic Zone, the Polar Frontal Zone and the Antarctic Zone. All zones are characterised by different temperatures, nutrient- and chlorophyll levels and salinities (Bostock et al., 2013). Due to these steep latitudinal gradients at the 3 fronts, movement of these fronts and therefore the ACC have consequences on upwelling, ice melting rates and CO_2 outgassing (Sokolov & Rintoul 2009; Meijers et al., 2011, Bostock et al., 2013). Most studies of frontal movements have focused on the Pleistocene, during which global ice volume changed strongly over glacial and interglacial cycles. During the Pliocene, this ice volume change was less profound, which raises the question of whether ocean frontal system movement was smaller in the Pliocene as well (Ballegeer et al., 2012).

The Pliocene epoch spans from 5.33 to 2.58 Ma (Gradstein et al., 2012). Even though the Pliocene is often regarded as an analogue for ongoing climate change (Vleeschouwer et al., 2018), climate records such as ice-volume records, the occurrence of IRD, as well as palynological and geochemical proxies in marine or terrestrial records show a significant climate variability over the time span of this period with an overall transition from warmer to cooler climate (Lisiecki & Raymo, 2005; Burke et al., 2018; Schepper & Chandler, 2009; De Schepper et al., 2014). An abrupt cooling episode reached its maximum at the globally recognisable glaciation event during Marine Isotopic Stage (MIS) M2 around 3.3 Ma (Dolan et al., 2015). This cooling period is seen as a premature attempt of the climate to establish a glacial state. The benthic $\delta^{18}O$ stack deepens steeply between 3.305-3.285 Ma with an amplitude shift of 0.64‰ (De Schepper et al., 2013; Dolan et al., 2015). Accompanying sea-level variations with a sea-level drop between 20-60 m imply the build-up of an ice sheet during that 50,000-year glaciation (Tan et al., 2017). The role of the Antarctic Ice Sheet during this transient glaciation is still being discussed. The M2 glaciation is mostly seen as a Northern Hemisphere glaciation and not many studies have

focused on the Antarctic ice sheet. However, first evidence was found that the ice sheet must have been more sensitive to climate change during the Pliocene than previously assumed (e.g. McKay et al., 2012; De Schepper et al., 2014).

The M2 glaciation was followed by the mid-Pliocene warm period (mPWP) starting at 3.264 Ma (Austermann et al., 2015). This period lasted until 3.025 Ma during which atmospheric CO_2 concentrations ranged between 350-450 ppm (Dolan et al., 2015; Haywood et al., 2016; de la Vega et al., 2020). Through the use of climate models, mean surface temperatures are estimated to have been 2.7-4.0°C higher than today (Haywood et al., 2016). During this interval, sea levels were 10- 20 meters higher compared to today which requires contributions from Greenland, West Antarctica and East Antarctica (De Schepper et al., 2013). As the contribution and the development of the Antarctic Ice Sheet throughout the Pliocene is still uncertain, the question arises of how the ocean conditions around Antarctica changed across the transient glaciation and the mPWP. In this study, we focus on understanding how ocean frontal systems migrated during the Pliocene.

For this, dinoflagellates will be used. Dinoflagellates are single-celled protists that predominantly live in marine surface waters and produce dinocysts during their lifecycle (Houben et al., 2013). The geographic distribution of these cysts is known through correlations of dinocyst assemblages in modern surface sediments and the ocean conditions in the overlying water (e.g., Sangiorgi et al., 2018; Prebble et al., 2013). It is assumed that these oceanographic affinities have remained the same within one species over time, therefore palaeoceanographic conditions of the past can be inferred from downcore dinocyst assemblages. Hence, dinocysts are a reliable proxy used to reconstruct marine paleoenvironments (Zonneveld et al., 2008).

We generate new palynological data (dinocyst assemblages) on 51 samples of IODP site 1168 and compile with available SST records of this site. With this data, qualitative palaeoceanographic conditions at the study site during the Pliocene are inferred by investigating how dinoflagellate communities responded to changing environmental conditions. As the site is located in an area where oceanic frontal systems migration can occur, in particular, conclusions about the migration of these fronts during the transition from colder (M2) to warmer (mPWP) periods are discussed. The offset between SST change and dinocyst assemblage response is compared with U1475 (Agulhas plateau).

3 Material and methods

3.1 Site description

International Ocean Discovery Program (IODP) Site 1168A is located on the 4° slope of the western margin of Tasmania, ~70 km west of the coast, at a water depth of 2463.3 m (middle bathyal) at 42°36.5809'S, 144°24.7620'E (Figure 1). During the Pliocene, Tasmania was located around 2° to the south compared to its modern position (Ballegeer et al., 2012).

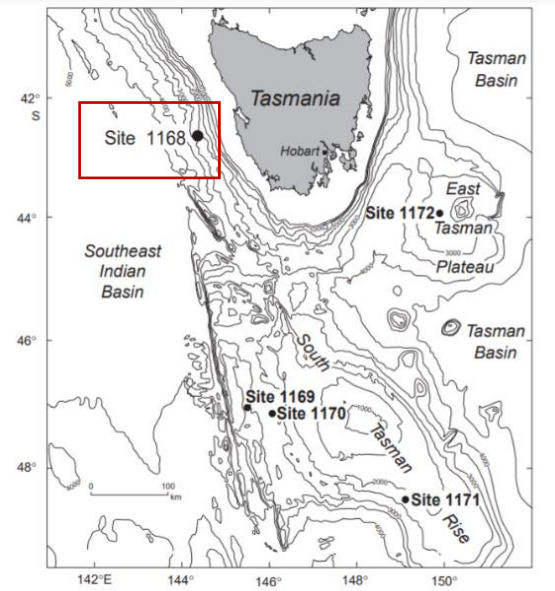

Figure 1 Location of IODP Site 1168 offshore west Tasmania (adapted from Exon et al., 2001).

In total, 883.5 m of sediment were cored using two hydraulic piston corer and 94.72% of the cored sediment was recovered, covering a time span from the early late Eocene to the present. The sediments used in this study consist of light greenish-grey foraminifer-bearing nannofossil ooze (Appendix B) and the sedimentation rates were calculated at 2-4 cm/ky). This site is located north of the present-day STF, making it the most dominant feature (Figure 2) (Stickley et al., 2004; Ballegeer et al., 2012).

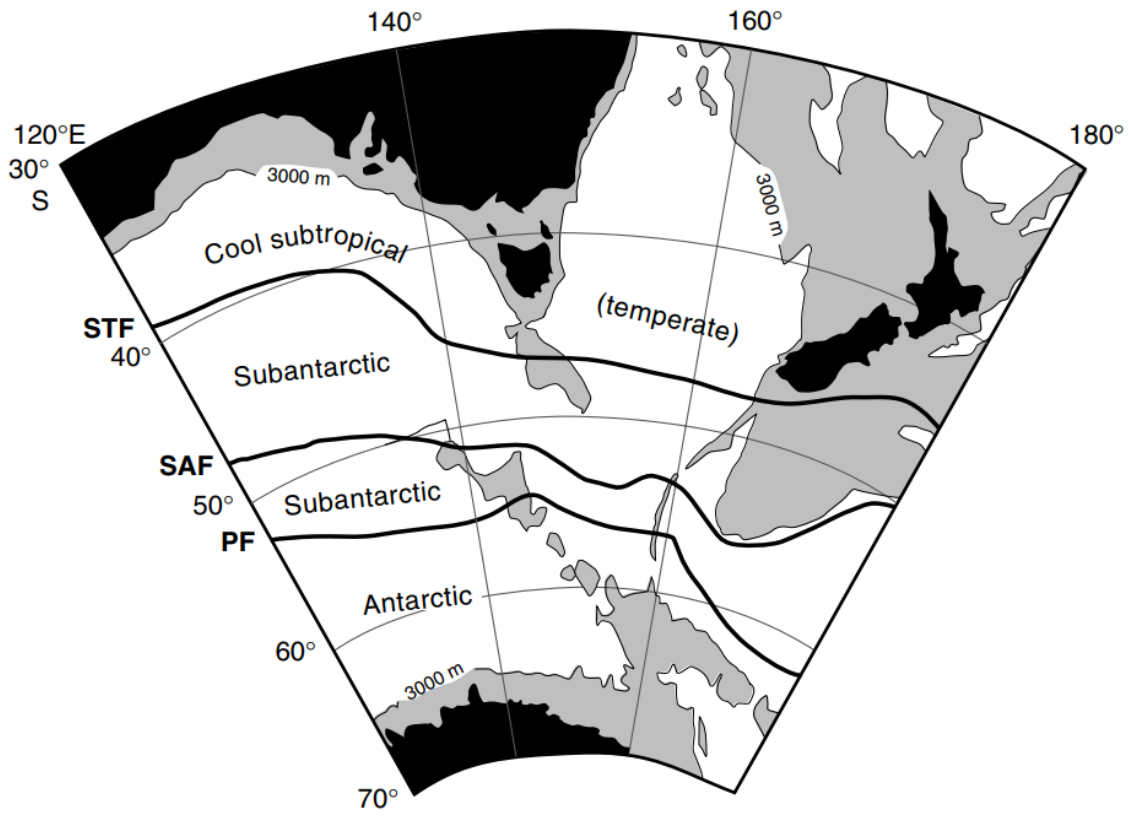

Figure 2 The oceanographic fronts in the Southern Ocean south of Tasmania today, STF = Subtropical Front; SAF = Subantarctic Front; and PF = Polar Front. After Rintoul and Bullister (1999).

3.2 Age model

An age model was provided which used the refined age model of Stickley et al. (2004) that was recalibrated to GTS2020. Their model improved the provisional onboard age model using higher-resolution diatom and dinocyst biostratigraphy, stable oxygen isotope stratigraphy and paleo-magnetostratigraphy. Age predictions for each sample are made in R by applying a loess fit curve (10% smoothing span) to calculate the depth of the samples. However, since the age model of the time interval of this study is only based on 3 magnetic reversals that were recognised in core B, a new age model was constructed. This was done by establishing tie points between the global $\delta^{18}O$ record provided by Lisiecki & Raymo (2005) and the colour stack of the core (Figure 3). This stack was calculated by adding up the standardised lightness, redness and greenness, L*, a* and b* respectively. The most distinctive tie point was the M2 event which can clearly be recognised in both records. A total of 21 tie points led to a new, improved age model (Figure 4).

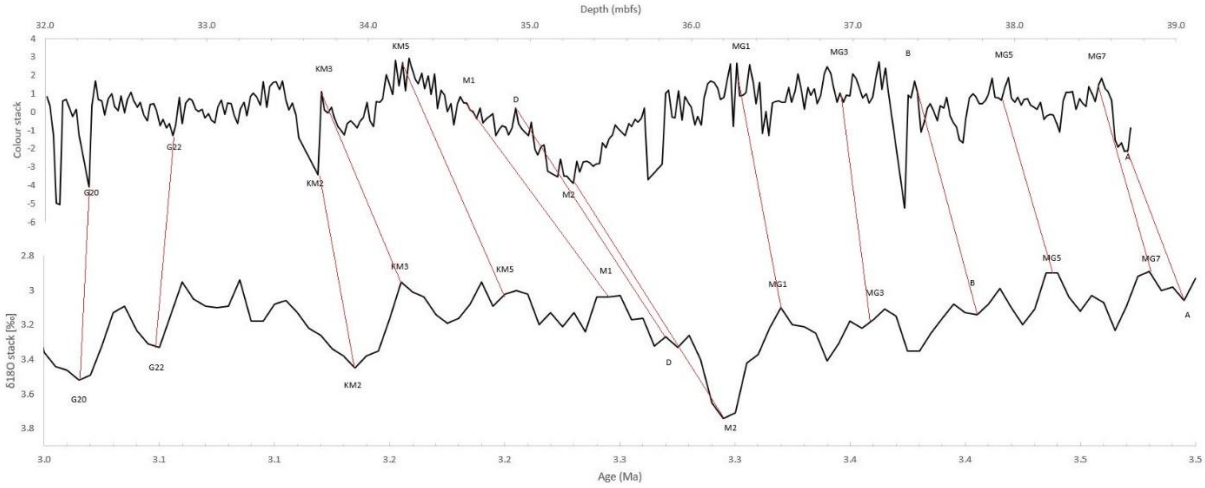

Figure 3 Tie points of the global $\delta^{18}O$ record and the colour stack used to construct the new age model. For points without an official name, letters in alphabetical order were used.

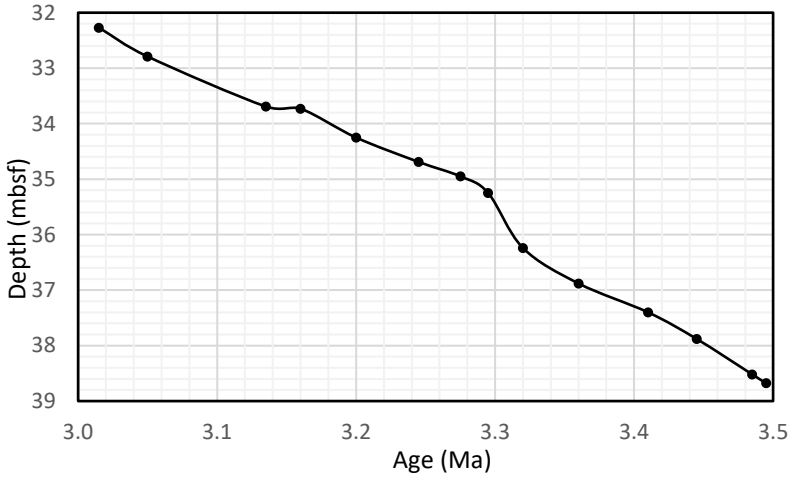

Figure 4 Improved age model for the mid-Pliocene section of IODP Site 1168A. Ages are calculated using linear interpolation between the 14 tie points.

3.3 Palynology

51 samples were previously processed and slides made prior to the start of this project, using standard palynological processing techniques at the Laboratory of Palaeobotany and Palynology at Utrecht University (e.g., Sluijs et al., 2003). In short, each sample was freeze-dried at 60°C and weighed. A known amount of lycopodium spores were added to allow the absolute quantification of dinocysts. Carbonate and silicate were removed with 30% hydrochloric acid (HCl) and 30% hydrofluoric acid (HF), respectively. To decant the supernatant after overnight settling, samples were shaken for 2 hours and again exposed to HF. After sieving the samples with a 10 µm mesh and exposing them to an ultrasonic bath, the residue of each sample was placed on a microscope slide with glycerine jelly.

All slides were counted on an Olympus CX21 light microscope at 200× and 400× magnifications to at least 200 dinocysts, as this number is sufficient for reliable relative abundance estimates. The

remainder of the slide was then scanned for rare species. When dealing with low yields, a minimum of 100 dinocysts were counted. Dinocysts were counted to a species level, if possible, whereas other palynomorphs were counted in broader categories, namely, trisiccate, bisiccate and other pollen, and cymatioshphaera. Simultaneously, lycopodium spores were counted.

3.4 Data analysis

After counting all 51 samples, a Principal Component Analysis (PCA) was performed in R on the identified species/genera. The aim of this analysis is the identification of dinocyst assemblages that show similar trends. Similar environmental affinities can thereby be assigned to each group. The resulting grouping was compared with the grouping found in Prebble et al. (2013), Zonneveld et al. (2013) and Brinkhuis (1994) to assess whether the grouping is in agreement with surface assemblages. The relative abundances found in different time periods throughout the record were furthermore assigned, if possible, to the clusters discussed in Thöle et al. (in review, 2022). They performed a *k*-means cluster analysis in order to investigate palaeoceanographic conditions from the dinocyst assemblages. The environmental grouping can be found in Table 1.

Table 1 Environmental grouping of the 39 species counted in the 51 samples.

Complex	**Dinocyst taxa**	**Ecological affinities**	**Reference**
Polysphaeridium cpx	*Polysphaeridium spp.* *Lingulodinium machaerophorum*	Inner-neritic setting	Prebble et al., 2013; Zonneveld et al., 2013
Other gonyaulacoid	*Pyxidonopsis reticulata* *Cerebrocysta* *Filisphaera* *Habibacycsta* *Tectatodinium* *Pentapharsodinium dalei* *Invertocysta tabulata* *Ataxiodinium spp.*	Outer-neritic setting	Brinkhuis, 1994; Sluijs et al., 2005
Spiniferites cpx	*Spiniferites bentorii* *S. elongatus* *S. membranaceus* *S. mirabilis* *S. ramosus* *S. splendidus* *S. spp.* *Achomosphaera spp.*	Cosmopolitan environment	Zonneveld et al., 2013

Complex	Dinocyst taxa	Ecological affinities	Reference
Other Operculodinium	*Operculod. janduchenei* *Operculod. Sp.1* *Operculod. eirikianum* *Operculod. israelinium*	Cosmopolitan/oceanic environment, North of STF	Brinkhuis, 1994; Prebble et al., 2013
Operculodinoium cpx	*Operculodinium centrocarpum* *Impagidinium aculeatum*	North of STF	Zonneveld et al., 2013
Other Impagidinium cpx	*Impag. pallidum* *Impag. paradoxum* *Impag. patulum* *Impag. sphaericum* *Impag. velorum*	Oligotrophic, oceanic	Prebble et al., 2013, Zonneveld et al., 2013
Nematosphaeropsis labyrinthus		Oceanic, South of STF	Prebble et al., 2013
Islandinium spp.		Temperate to polar distribution, Low salinity	Sluijs et al., 2005; Zonneveld et al., 2013
Protoperidinioid cpx	*Brigantedinium spp.* *Echinidinium spp.* *Selenopemphix quanta*	Nutrient-rich cold waters, related to inner-neritic environments	Prebble et al., 2013

4 Results

There is a clear trend of a decreasing relative abundance of dinocysts compared to the acritarchs (*Cymatiosphaera*) and the terrestrial palynomorphs towards the younger samples (Figure 5). While in the older samples dinocysts make up ~75% of the total palynomorphs, in the younger samples that number decreases to ~10%. Simultaneously, the opposite trend can be recognised in the relative abundance of *Cymatiosphaera* (from 40% to 90%). The terrestrial palynomorphs are constantly minor, even though that number decreases slightly towards the younger samples.

In total, 34 dinocyst species were identified throughout all samples (Appendix A). For some individuals, only the genus level could be identified which was the case for 5 genera. The main genera in all slides were *Impagidinium*, *Nematosphaeropsis*, *Operculodinium* and *Spiniferites*. In every sample, they represent at least 74% of the total dinocysts.

The record shows 4 distinctive changes in dinocyst assemblages at ~3.3, ~3.2, ~3.1 and ~3.03 Ma (Figure 5). In the interval between 3.49-3.3 Ma (38.71-35.54 mbsf), the *O. centrocarpum complex* dominates with high relative abundances. The *Polysphaeridium*, the *Spiniferites*, the other *Impagidinium* and the other *Operculodinium* complexes also show high abundances during this period. Contrary to this, showing low relative abundances are the other Gonyaulacoid complex and *N. labyrinthus*. The relative abundances of these dinocyst complexes correspond to the Iacu-Cluster discussed in Thöle et al. (in review, 2022).

From 3.3 Ma on, which coincides with the onset of the MIS M2 glaciation, until 3.2 Ma (35.54-34.3 mbsf) these abundances are the exact opposite. The abundance of *N. labyrinthus* increases significantly while the *O. centrocarpum complex* reaches its minimum relative abundance throughout the whole record, therefore corresponding to the Nlab-Cluster of Thöle et al. (in review, 2022). Simultaneously, the other *Impagidinium*, other *Operculodinium*, and *Spiniferites* complex increase and subsequently decrease towards the end of this period. *Islandinium* spp. occurs for the first time, but quickly disappears again.

During the interval between 3.2 and 3.1 Ma (34.3-33.39 mbsf), the *O. centrocarpum complex* recovers its high abundance which coincides with a drop in *N. labyrinthus*. Interestingly, even though it seemed to mirror its relative abundance in the periods before, the other Gonyaulacoid complex is increasing throughout this period after an initial drop in relative abundance around 3.1 Ma. Just like the first phase, this cluster is in agreement with the Iacu-Cluster described in Thöle et al. (in review, 2022).

From 3.1 until 3.03 Ma (33.39-32.51 mbsf), the same pattern that was observed in the second period is repeated. However, the environmental conditions seem to have increased in favour of *N. labyrinthus* and the *Spiniferites* complex, and at the expense of all other complexes.

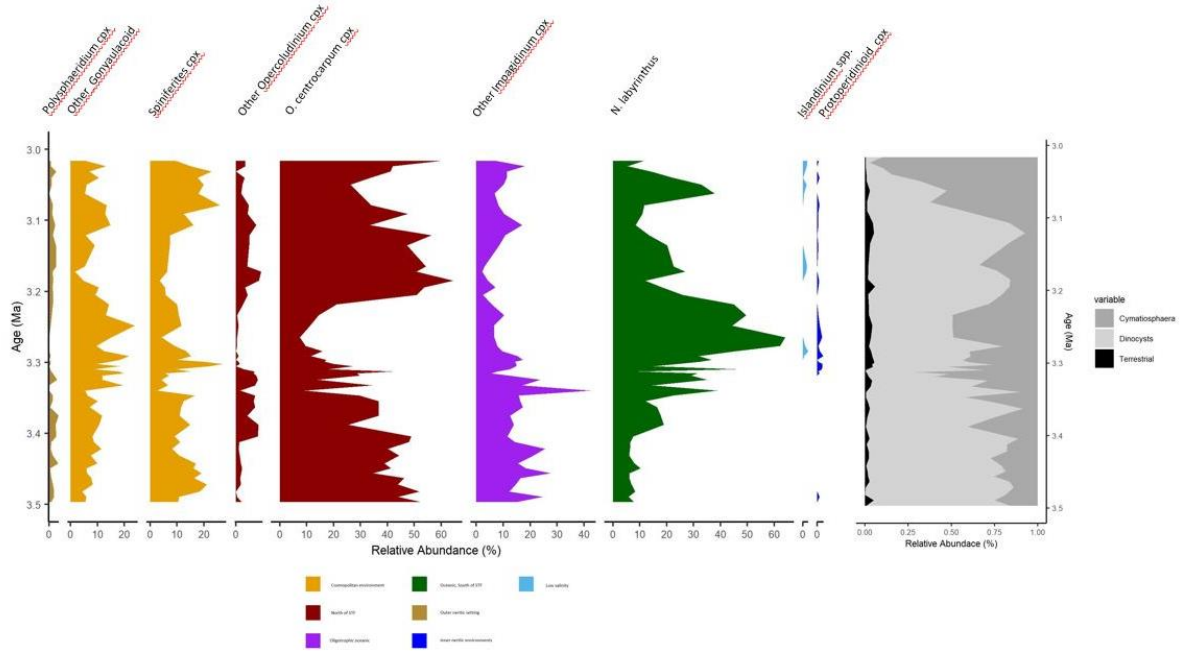

Figure 5 Relative abundance of the dinocyst groups, ordered according to their environmental occurrence. On the right, the relative abundances of Cymatiosphaera, dinocysts and terrestrial palynomorphs are shown.

From this distinctive pattern of lower and higher abundances of complexes and the fact that some of them seem to behave similarly, it is clear that the patterns observed are the results of different environmental conditions throughout the record. This becomes especially clear by the opposing behaviour of the two dominant complexes *O. centrocarpum* and *N. labyrinthus*. By comparing their ecological affinities, two periods characterised by colder conditions between 3.3-3.2 Ma and 3.1- 3.03 Ma can be pinpointed. These are interrupted by a warm interval between 3.2 and 3.1 which coincides with the mPWP, as well as a warm interval prior to the cooling the location experienced at 3.3 Ma.

5 Discussion

5.1 Environmental reconstruction

A general oligotrophic environment is suggested by the dominance of *Impagidinium*, *Nematosphaeropsis*, *Operculodinium* and *Spiniferites*. This is also supported by the low counts of Protoperidiniod cysts throughout the record. Even though *N. labyrinthus* is found in oligotrophic and eutrophic environments, the highest abundances are observed in areas with low upper-water productivity (Zonneveld et al., 2013). Some *Spiniferites* species are also found in both oligotrophic and eutrophic environments, but as their counts are relatively low, not too much focus will be placed on them.

For this core, TEX_{86}-based SST data (Hou, personal communication) are available (Figure 7). An SST-H calibration following Kim et al. (2010) was used. The known temperature affinities of the dinocyst assemblages can therefore be compared with the reconstructed SST record of this core. Generally, warmer environmental conditions are accompanied by high abundances of the Polyshphaeridium complex, the *Spiniferites* complex, the other O*perculodinium* complex, the *O. centrocarpum complex* and the other *Impagidinium* complex which correspond to the Iacu-Cluster discussed in Thöle et al. (in review, 2022). The SST record during the times when these complexes dominate shows average temperatures of 18°C. Colder temperatures (on average 13°C in the SST record) however are documented during periods in which *N. labyrinthus* and the Protoperidinioid complex are dominant (Nlab-Cluster of Thöle et al. (in review, 2022)). This observation is in agreement which similar studies such as Hoem et al. (2021) and Prebble et al. (2013).

During the lower part of the record, that is dominated by the warm-affiliated *O. centrocarpum* complex, therefore suggesting warmer temperatures, a sudden peak in *N. labyrinthus* at 3.38 Ma is visible. This peak coincides with the MG2 event and is accompanied by a sudden decline in the relative abundance of the *O. centrocarpum* complex. Towards the top of the period, short alternations in peaks between the two complexes suggest changing environmental conditions towards a colder interval during M2.

A strong cooling with the start of M2 is suggested by the increasing relative abundance of *N. labyrinthus* and the accompanying low abundances of the *O. centrocarpum* complex. The response of *N. labyrinthus to* these cooler conditions reaches its maximum at 3.27 Ma. A simultaneous increase in the abundance of the Protoperidinioid complex implies nutrient-rich, productive surface waters at that time (Hoem et al., 2021).

The mPWP starting at 3.26 Ma is demonstrated in the record by the shift in dominance towards the *O. centrocarpum* complex. Even though the mPWP reaches from 3.26 to 3.025 Ma, the record suggests a

second colder interval with a peak in *N. labyrinthus* abundance at 3.0623 Ma which might correspond to G22. However, the peak is less strong than during M2 and the period is shorter, suggesting that this interval was significantly warmer than M2.

Throughout the whole record, the other Gonyaulacoid complex does not seem to follow a certain pattern. During the first, warmer part of the record, its relative abundance is higher, therefore implying that this complex follows the general trend of the *O. centrocarpum* complex. However, with the start of M2, at times it also seems to follow the trend of *N. labyrinthus*. This could be attributed to the low counts of all dinocyst species contributing to this complex.

To conclude, the SST reconstructions are very consistent with the temperatures that belong to the dinocyst assemblages and therefore also with the corresponding temperatures of the two clusters that are discussed in Thöle et al. (in review, 2022). The study site experienced a great variability in SST and therefore in dinocyst assemblage in the Pliocene.

It is important to keep in mind that dinocysts may be exposed to lateral transport and relocation after deposition due to water transport and bottom currents (Nooteboom et al., 2019). Especially in the SO, water masses are transported by strong upper-level currents and fast bottom-water currents (Esper & Zonneveld, 2002). Through this transport, local dinocyst assemblages may be altered. However, as all trends in the dinocyst assemblages can be explained by changes in environmental factors, it is not assumed that the dinocyst encountered during this study were exposed to transport or relocation.

Regarding other palynomorphs, of particular interest are the sudden increase in *Cymatiosphaera* and the simultaneous decrease in dinocyst abundance at the top of the record (3.04-3.01 Ma). Generally, the occurrence of *Cymatiosphaera* indicates freshwater influx, normal to low salinity, nutrient-rich surface waters, or surface water stratification (Hartman et al., 2021; Wrenn et al., 1998; Mudie et al., 2011). A freshwater influx, however, is unlikely, since the study area is not located close to any rivers or major meltwater sources during this period. Interestingly, this sudden peak appears after an increase in the relative abundance of *N. labyrinthus*. This may point towards a delayed response of the *Cymatiosphaera* bloom to changing ocean conditions such as an intensification of nutrient-rich surface waters. However, it does not explain, why this delayed reaction does not occur during the even more pronounced peak of *N. labyrinthus* during M2.

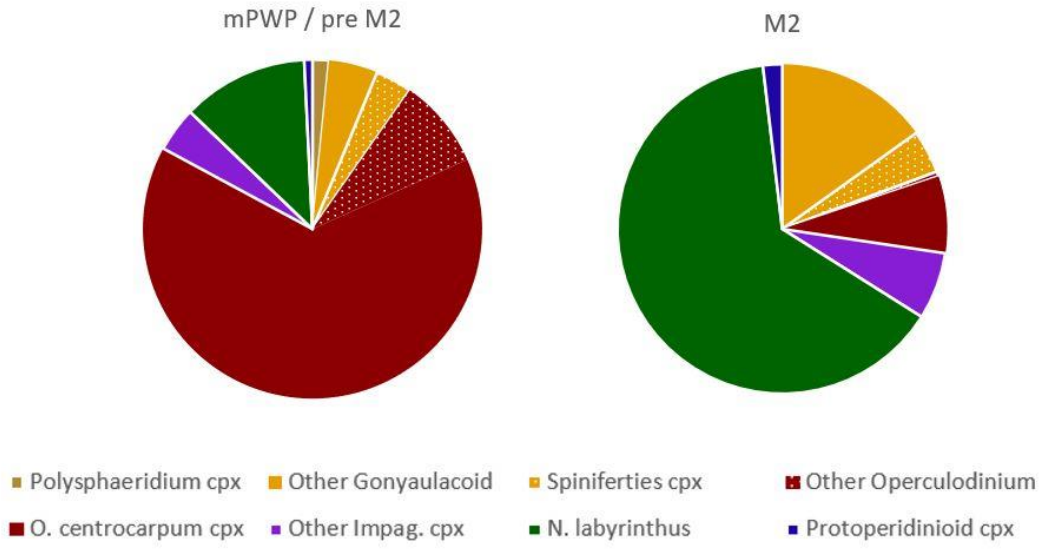

Figure 6 Representative dinocyst assemblage abundance during M2 and mPWP/pre M2. While M2 is dominated by N. labyrinthus, mPWP/pre M2 shows high relative abundance in the O. centrocarpum complex. The maximum dinocyst assemblage responses were chosen to highlight the different assemblages.

5.2 Offset between SST change and dinocyst signal

The dinocyst assemblages generally show a positive correlation with the TEX_{86}-based SST data (Hou, personal communication) (Figure 7). Several events such as the M2 are clearly recognisable. The SST data also verifies the environmental reconstruction using the dinocyst assemblages described in 5.1. There is a clear correlation between temperature change and dinocyst assemblage change. Of particular interest is the lagged response of the assemblages to SST. Temperatures gradually decreased with the start of M2 which established optimum conditions for a dinocyst assemblage dominated by *N. labyrinthus*. Temperatures started to decline from 3.312 Ma on and the lowest temperatures were reached at 3.29 Ma. At 3.302 Ma, the relative abundance of *N. labyrinthus* started to increase and reached its maximum at 3.264 Ma. This means that there is an offset between 10 and 33 ka between declining temperatures and increasing abundance. Not much research has been done on how long the period between changing environmental conditions and the resulting alternation in dinocyst assemblage is. A possible explanation for the delayed dinocyst assemblage response might be that the dinocysts responded not to changing temperatures but to changing salinities during this period. The deglaciation of M2 results in a freshwater input released from the melting Antarctic ice sheet and icebergs. This influx may have triggered this peak in *N. labyrinthus*. Thoele et al. (in review, 2022) show an average salinity of 34.4 psu in the Nlab cluster which is slightly lower than the average salinity in the Iacu cluster (35.5 psu). This further supports this theory.

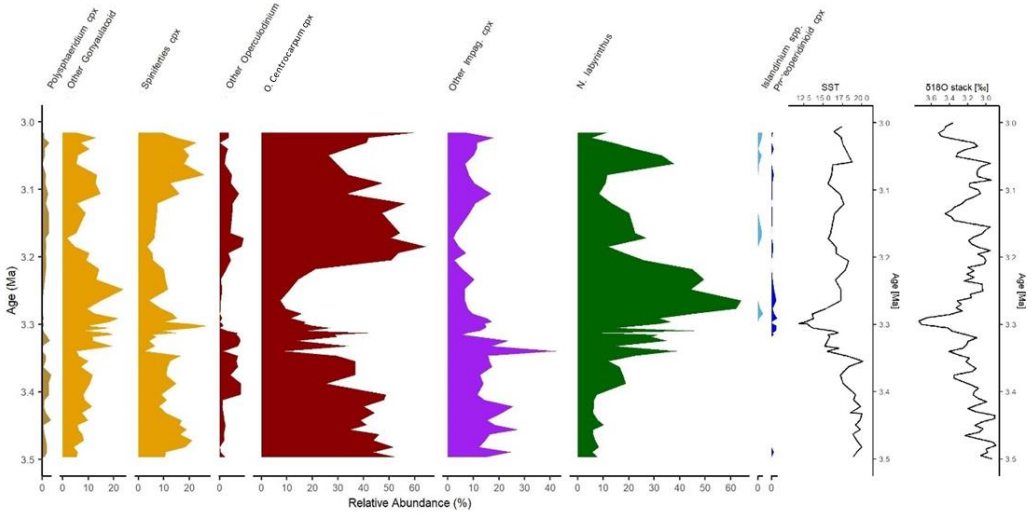

Figure 7 Relative abundance of the dinocyst groups, ordered according to their environmental occurrence. On the right, the SST record of this site and the global $\delta^{18}O$ stack adapted from Lisiecki & Raymo (2005) are plotted.

5.3 Frontal shifts

To the north, the STF is restricted by the Leeuwin Current (LC) which is a surface current that flows poleward and transports warm, low-salinity waters (He et al., 2021; De Vleeschouwer et al., 2019). A strengthening of this current would result in warmer water flowing more to the south and thereby a southward movement of the STF. The opposite is expected during a weakening of the LC. To assess shifts in the position of the STF, dinocyst assemblages during cold and warm intervals of the record were compared to similar studies (e.g., Prebble et al., 2013; Esper & Zonneveld, 2002; Hoem et al., 2021), to the SST and $\delta^{18}O$ record. The generated data suggests latitudinal migration of the STF towards the north and the south over the study interval.

The main indicator species for a location in and south of the STF is *N. labyrinthus* while a location north of the STF is mainly indicated by the dominance of the *O. centrocarpum* complex and the other *Operculodinium* complex (Zonneveld et al., 2013; Prebble et al., 2013) (Figure 6).

The short alterations in peaks between the *O. centrocarpum* complex and *N. labyrinthus* at 3.34-3.305 Ma suggest that the STF moved closer to the study site. This would bring different water masses to this location, thereby providing favourable environmental conditions for both complexes (Prebble et al., 2013)

The increase in colder-affiliated *N. labyrinthus* from the start of M2 (3.3 Ma), is a direct result of colder temperatures, which is most likely linked to a northwards movement of the STF with respect to the study site during this period. Subsequently, the increased abundance of warm-water species, indicating warmer temperatures reaching the study area around 3.23 Ma would require a poleward

shift of the STF. This timing coincides with the mPWP. The response to these warmer temperatures is represented by a decrease in *N. labyrinthu*s and a simultaneous increase of the *O. centrocarpum*, other *Operculodinium* and Polysphaeridium complex.

A second northwards movement of the STF can be inferred from the assemblage between 3.06 and 2.9 Ma. The same assemblages as seen during the M2 are present here with high relative abundances of *N. labyrinthus* and the *Spiniferites* complex. However, as the relative abundance of these species compared to the others are not as low as during 3.3 Ma, it can be inferred, that the STF did not move as much northwards as before. This is further supported by the relative abundance of all other complexes, which are higher than at 3.3 Ma.

By comparing the different dinocyst assemblages north and south of the STF, an indication of how much this latitudinal migration was, can be given. Prebble et al. (2013) provide assemblage results of the *k*-means cluster analysis. Given that the *N. labyrinthus* complex is corresponding to Cluster 3 and that the *O. centrocarpum* complex is corresponding to Cluster 4, a latitudinal migration of ~3-4° of the STF can be inferred between the maximum southernmost (mPWP) and the maximum northernmost position (M2). This is comparable to the latitudinal change of the STF during the Pleistocene on a glacial-interglacial scale, as described in Bostock et al. (2015).

A northward movement of the STF due to declining SST and a weakening of the East Australian and the LC Current enhances upwelling conditions, especially along the shelf edge. This in turn leads to less stratified ocean conditions (Gallagher et al., 2003). This explains the higher abundance of heterotrophic species (Protoperidinioid complex) during periods that were characterised by a northward migration of the STF. Furthermore, can the exchange of heat and salt fluxes by the AMOC, which exchanges surface water along a warm and cold route, be altered by a migration of the STF in the SO (Bard & Rickaby, 2009).

To conclude, there has been a significant latitudinal shift of the STF before, during and after the M2 that is recorded in the dinocyst assemblage. Such latitudinal migrations are commonly associated with the expansion and contraction of the sea ice. This, in return, is evident for a dynamic ice sheet that was sensitive to changes in SST before, during and after the M2 event. Therefore, it can be concluded that the Antarctic ice sheet experienced more waxing and waning during the Pliocene than previously assumed. This is further supported by the results of Dwyer & Chandler (2009), who suggest a sea-level variation of 25 m above and 25 m below modern-day sea level during the mPWP. These changes required contributions from Antarctica, in particular, the East Antarctic Ice Sheet (EAIS) must have significantly retreated (De Schepper et al., 2014). During KM5, KM3, K1 and G17 as much as 25-30% of that built-up ice must have melted in order to contribute to such a sea-level change (De Schepper et

al., 2014). Similar values for a sea-level change during the mPWP were calculated by Raymo et al. (2018) who estimated 23 m of sea level equivalent to be lost from Antarctica during the mPWP. However, uncertainty is given by the fact that such a significant amount of ice sheet was lost without simultaneous bottom-water warming (Raymo et al., 2018).

5.4 Comparison with IOPD Site U1475

IODP Site U1475 is located ~450 nautical miles south of South Africa on the Agulhas plateau. Stockhausen (2022, unpublished) counted dinocysts in 33 samples following the same methods described in 4.3. The results show a pronounced increase in *Cymatiosphaera* and a simultaneous decrease in dinocyst counts. Interesting is however, that the timings of increase at U1475 and 1168 do not coincide. The increase in *Cymatiosphaera* in U1475 starts at 3.229 Ma and peaks at around 3.2116 Ma (Figure 8). At site 1168, *Cymatiosphaera* increase at 3.0907 Ma and peak at 3.0238. After this, they seem to decline again, however, because there is no more data available after that time, this remains unsure. Also, the time period during which *Cymatiosphaera* dominate in both cores does not coincide. The fact that both sites are located very distant from each other and that they are therefore exposed to different oceanographic environmental parameters leads to the conclusion that the *Cymatiosphaera* increases are not related to changing global- but to very local conditions that laterally cannot be correlated. Local icebergs in U1475 and their subsequent melting could cause a *Cymatiosphaera* bloom. These local factors responsible for the increase may however be the same at both locations during both periods. In core U1475 as well as in core 1168 an increase in *N. labyrinthus* precedes the high relative abundances of *Cymatiosphaera*. As *Cymatiosphaera* are indicators for nutrient-rich surface waters, their increase may be a delayed reaction to the northward movement of the STF, as this movement enhances upwelling conditions (see 6.3).

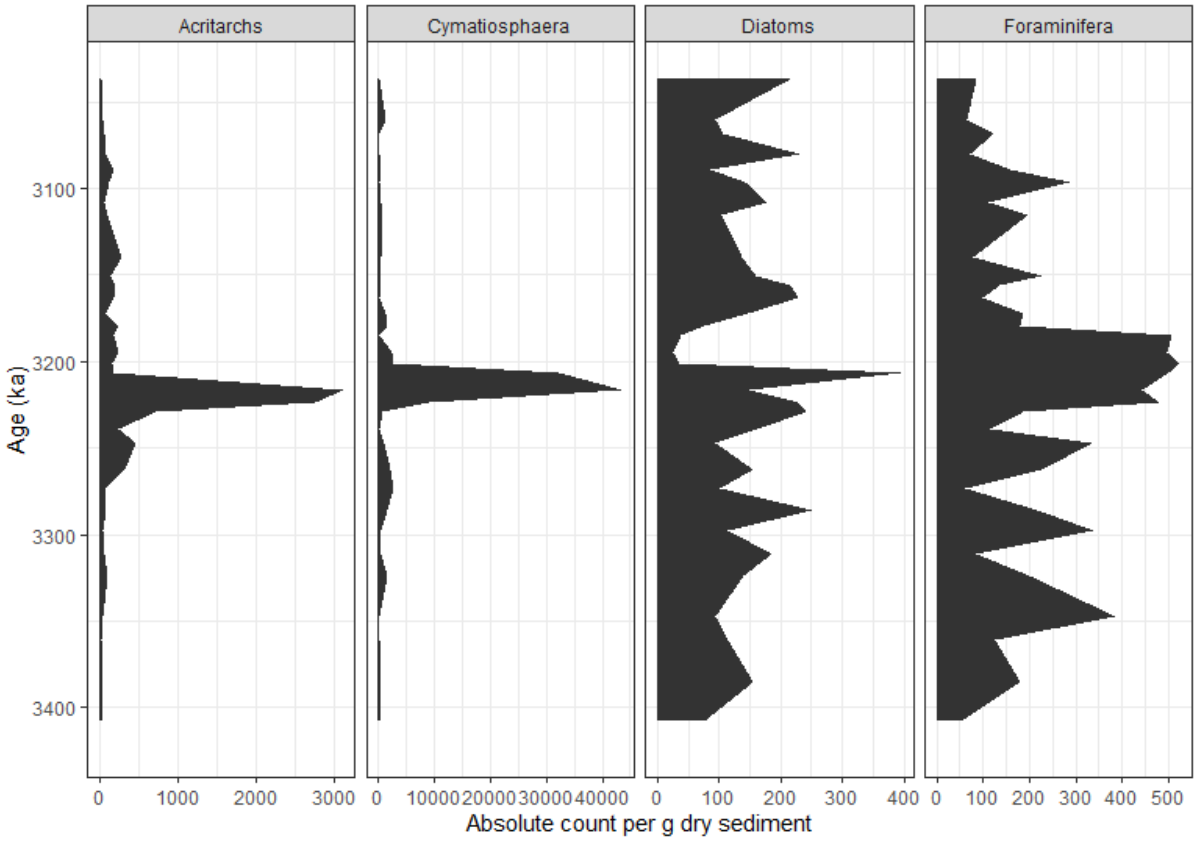

Figure 8 Absolute counts of Acritarchs, Cymatiospheara, pyritized Diatoms, and Foraminifera linings per g dry sediment in U1475. After Stockhausen (2022, unpublished).

Furthermore, Stockhausen (2022, unpublished) also encountered an offset between SST- and the global $\delta^{18}O$ stack (Figure 9). The SST record seems to either lag or precede distinct isotope stages. This is most notably around the M2 event, where temperatures seem to decrease ~16 kys before the 3.3 Ma mark. The global $\delta^{18}O$ stack however shows the most positive values after 3.3 Ma (Figure 9). It is uncertain whether these temperature offsets are a consequence of incorrect tuning of the age model. Stockhausen (2022, unpublished) furthermore discusses the possibility of the influence that icebergs that travelled to U1475 could have on surface temperature. This would lead to much colder temperatures reaching the study area prior to the start of M2. A similar premature SST drop was encountered in IODP Site 1087.

The uncertainty of the cause for this offset makes it difficult to compare the timing of SST- and dinocyst assemblage change between IODP Site U1475 and 1168. Even though the temperatures start to decline before the start of M2, an increase in *N. labyrinthus* is observed only after 3.3 Ma (Figure 9). The abundance of *N. labyrinthus* even declines from 3.32 to 3.3 Ma. The offset between minimum temperatures and highest *N. labyrinthus* abundance is ~30 ka in U1475 which is comparable to the observed offset in 1168. However, since not much research has been done on the timing of dinocyst

assemblage response on the temperature change, a comparison with more sites is necessary to draw reasonable conclusions.

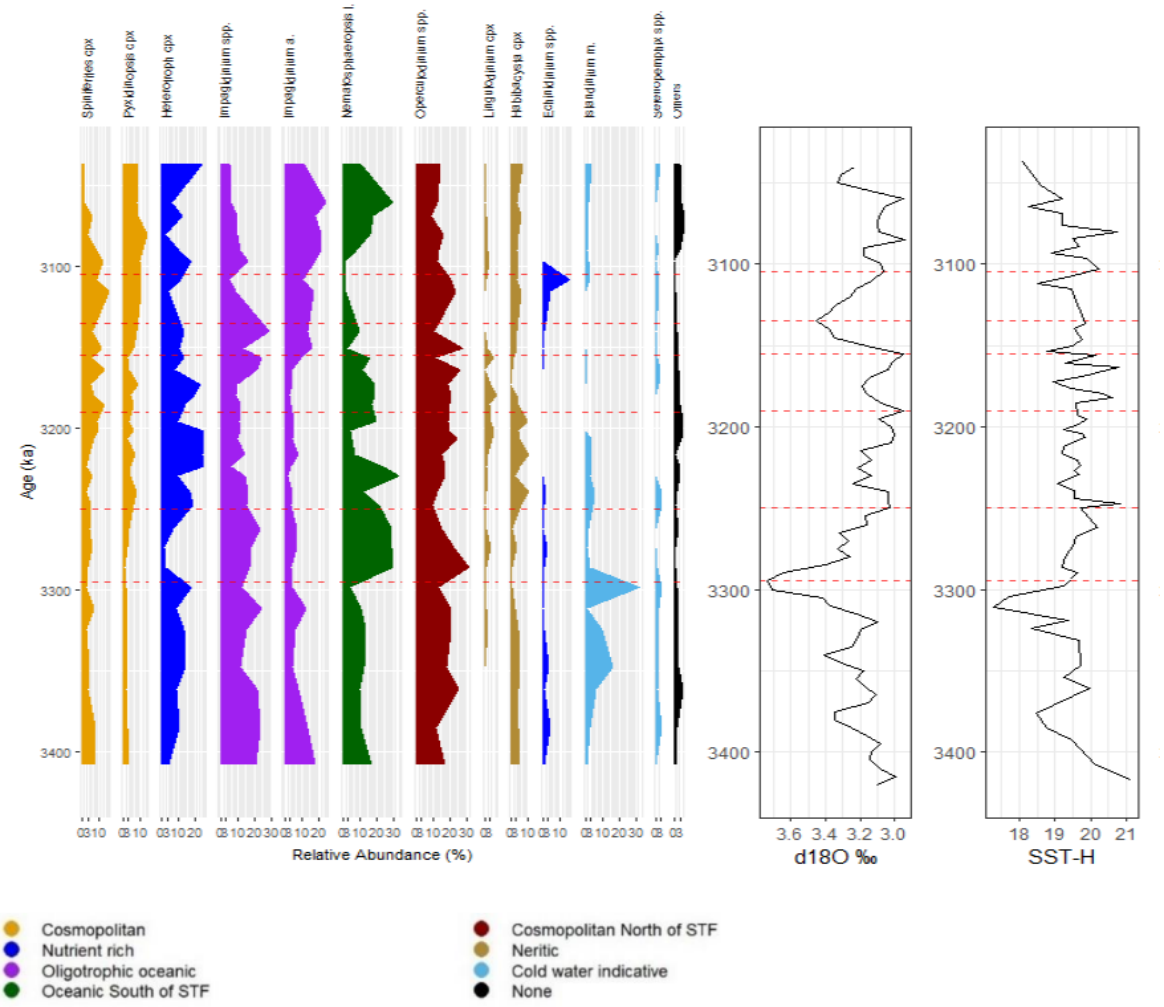

Figure 9 Relative abundance of dinocyst groups/taxa of U1475 ordered according to their environmental occurrence, and on the right the global $\delta^{18}O$ stack adapted from Lisiecki & Raymo (2005), and the Tex_{86} based SST reconstruction of this site. After Stockhausen, 2022 (unpublished).

5.5 Comparison with other sites

McKay et al. (2012) analysed diatom assemblages from core ANDRILL AND-1B beneath the Ross Ice Shelf. They further reconstructed SST based on TEX_{86} data. Their results show that the Ross Sea experienced cooling SST from 3.3 Ma on, which resulted in the expansion of an ice sheet into the Ross Sea and a simultaneous stepwise expansion of sea ice. This sea ice limited the influence of warmer water through the northward migration of ocean fronts. These conclusions are in agreement with the results found during our study.

A northward migration of the STF during the M2 glaciation is also suggested by McClymont et al. (2016) who observed an SST cooling trend at DSDP 593 and ODP 1125 from 3.1 Ma. This is also supported by changes in the diatom assemblage recorded at DSDP Site 513 and ODP Site 689 from 3.7 Ma on as

discussed in Kato (2020). Even though there is no diatom record of Site 513 younger than 5.3 Ma, sea ice expanded most likely until 3 Ma. This northward shift of the STF during M2 was also recognised in the nannofossil assemblage of ODP Site 1172 (Ballegeer et al., 2012).

A more dynamic ice sheet during the Pliocene has also been proposed by other studies in the SO. The decreased amount of IRD recorded in ODP Leg 1165 between 4.6-4.0 Ma is evident for a decreased extent of the EAIS (Passchier, 2011). An increase in IRD from 3.3 Ma on has been recorded off Prydz Bay (IODP 1165) pointing towards a major glacial advance of the EAIS during M2 (Passchier, 2011). Cook et al. (2013) provide evidence from Site U1361 for a dynamic EAIS and a major retreat of the ice sheet margin inland during peak Pliocene warm periods. This is further supported by Whitehead et al. (2001) that interpret the deposition of aeolian sediments in the Sørsdal Formation as evidence for an ice margin retreat.

6 Conclusion

We used dinocyst assemblages from core 1168, on the western margin of Tasmania, to reconstruct ocean conditions and latitudinal migration of the STF during the mid-Pliocene. The dinocyst assemblages suggest a strong surface oceanographic response of the STF during glacial-interglacial cycles in the mid-Pliocene. Our data showed that during the M2, the STF moved equatorward and during the mPWP, poleward. These results are in agreement with similar studies of nearby sites (e.g., Ballegeer et al., 2012; Passchier, 2011). Therefore, we could link a more dynamic Antarctic Ice Sheet than previously assumed to this latitudinal migration of the STF. By comparing the dinocyst assemblage with TEX_{86} derived SST data of this core, we observed an offset between changing temperatures and the response of the dinocyst assemblage. This was interpreted to be the dinocysts reacting to the freshwater influx related to the M2 deglaciation. This study demonstrates that by using dinocyst assemblages in combination with SST data, local palaeoceanographic reconstructions can be made, therefore supporting dinocysts to be a reliable proxy. Our data documents how the Antarctic Ice Sheet responded dynamically to changing Pliocene climatic conditions, therefore, indicating how vulnerable the ice sheet is to the current unequivocally global warming. Thus, this stresses the importance of researching how the polar ice caps responded to a warming world.

7 References

Austermann, J., Pollard, D., Mitrovica, J. X., Moucha, R., Forte, A. M., DeConto, R. M., ... & Raymo, M. E. (2015). The impact of dynamic topography change on Antarctic ice sheet stability during the mid-Pliocene warm period. *Geology*, *43*(10), 927-930.

Ballegeer, A. M., Flores, J. A., Sierro, F. J., & Andersen, N. (2012). Monitoring fluctuations of the Subtropical Front in the Tasman Sea between 3.45 and 2.45 Ma (ODP site 1172). *Palaeogeography, Palaeoclimatology, Palaeoecology*, *313*, 215-224.

Bard, E., & Rickaby, R. E. (2009). Migration of the subtropical front as a modulator of glacial climate. *Nature*, *460*(7253), 380-383.

Bostock, H. C., Barrows, T. T., Carter, L., Chase, Z., Cortese, G., Dunbar, G. B., ... & Armand, L. K. (2013). A review of the Australian–New Zealand sector of the Southern Ocean over the last 30 ka (Aus-INTIMATE project). *Quaternary Science Reviews*, *74*, 35-57.

Bostock, H. C., Hayward, B. W., Neil, H. L., Sabaa, A. T., & Scott, G. H. (2015). Changes in the position of the Subtropical Front south of New Zealand since the last glacial period. *Paleoceanography*, *30*(7), 824-844.

Brinkhuis, H. (1994). Late Eocene to Early Oligocene dinoflagellate cysts from the Priabonian type-area (Northeast Italy): biostratigraphy and paleoenvironmental interpretation. *Palaeogeography, palaeoclimatology, palaeoecology*, *107*(1-2), 121-163.

Burke, K. D., Williams, J. W., Chandler, M. A., Haywood, A. M., Lunt, D. J., & Otto-Bliesner, B. L. (2018). Pliocene and Eocene provide best analogs for near-future climates. *Proceedings of the National Academy of Sciences*, *115*(52), 13288-13293.

Chapman, C. C., Lea, M. A., Meyer, A., Sallée, J. B., & Hindell, M. (2020). Defining Southern Ocean fronts and their influence on biological and physical processes in a changing climate. *Nature Climate Change*, *10*(3), 209-219.

Cook, C. P., Van De Flierdt, T., Williams, T., Hemming, S. R., Iwai, M., Kobayashi, M., ... & Yamane, M. (2013). Dynamic behaviour of the East Antarctic ice sheet during Pliocene warmth. *Nature Geoscience*, *6*(9), 765-769.

De La Vega, E., Chalk, T. B., Wilson, P. A., Bysani, R. P., & Foster, G. L. (2020). Atmospheric CO2 during the Mid-Piacenzian Warm Period and the M2 glaciation. *Scientific Reports*, *10*(1), 1-8.

De Schepper, S., Gibbard, P. L., Salzmann, U., & Ehlers, J. (2014). A global synthesis of the marine and terrestrial evidence for glaciation during the Pliocene Epoch. *Earth-Science Reviews*, *135*, 83-102.

De Schepper, S., Groeneveld, J., Naafs, B. D. A., Van Renterghem, C., Hennissen, J., Head, M. J., ... & Fabian, K. (2013). Northern hemisphere glaciation during the globally warm early late Pliocene. *PloS one*, *8*(12), e81508.

De Vleeschouwer, D., Petrick, B. F., & Martínez-García, A. (2019). Stepwise weakening of the pliocene Leeuwin current. *Geophysical Research Letters*, *46*(14), 8310-8319.

Dolan, A. M., Haywood, A. M., Hunter, S. J., Tindall, J. C., Dowsett, H. J., Hill, D. J., & Pickering, S. J. (2015). Modelling the enigmatic late Pliocene glacial event—Marine Isotope Stage M2. *Global and Planetary Change*, *128*, 47-60.

Dwyer, G. S., & Chandler, M. A. (2009). Mid-Pliocene sea level and continental ice volume based on coupled benthic Mg/Ca palaeotemperatures and oxygen isotopes. *Philosophical Transactions of the Royal Society A: Mathematical, Physical and Engineering Sciences*, *367*(1886), 157-168.

Esper, O., & Zonneveld, K. A. (2002). Distribution of organic-walled dinoflagellate cysts in surface sediments of the Southern Ocean (eastern Atlantic sector) between the Subtropical Front and the Weddell Gyre. *Marine Micropaleontology*, *46*(1-2), 177-208.

Exon, N. F., Kennett, J. P. & Malone, M. J. (2001). 189. Proceedings of the Ocean Drilling Program, Initial Reports.

Gallagher, S. J., Greenwood, D. R., Taylor, D., Smith, A. J., Wallace, M. W., & Holdgate, G. R. (2003). The Pliocene climatic and environmental evolution of southeastern Australia: evidence from the marine and terrestrial realm. *Palaeogeography, Palaeoclimatology, Palaeoecology*, *193*(3-4), 349-382.

Gille, S. T., McKee, D. C., & Martinson, D. G. (2016). Temporal changes in the Antarctic circumpolar current: Implications for the Antarctic continental shelves. *Oceanography*, *29*(4), 96-105.

Gradstein, F. M., Ogg, J. G., Schmitz, M., & Ogg, G. (Eds.). (2012). *The geologic time scale 2012*. elsevier.

Graham, R. M. (2014). *The role of Southern Ocean fronts in the global climate system* (Doctoral dissertation, Department of Geological Sciences, Stockholm University).

Graham, R. M., & De Boer, A. M. (2013). The dynamical subtropical front. *Journal of Geophysical Research: Oceans*, *118*(10), 5676-5685.

Hartman, J. D., Sangiorgi, F., Barcena, M. A., Tateo, F., Giglio, F., Albertazzi, S., ... & Asioli, A. (2021). Sea-ice, primary productivity and ocean temperatures at the Antarctic marginal zone during late Pleistocene. *Quaternary Science Reviews*, *266*, 107069.

Haywood, A. M., Dowsett, H. J., & Dolan, A. M. (2016). Integrating geological archives and climate models for the mid-Pliocene warm period. *Nature communications*, *7*(1), 1-14.

He, Y., Wang, H., & Liu, Z. (2021). Development of the Leeuwin Current on the northwest shelf of Australia through the Pliocene-Pleistocene period. *Earth and Planetary Science Letters*, *559*, 116767.

Hoem, F. S., Sauermilch, I., Hou, S., Brinkhuis, H., Sangiorgi, F., & Bijl, P. K. (2021). Late Eocene–early Miocene evolution of the southern Australian subtropical front: a marine palynological approach. *Journal of Micropalaeontology*, *40*(2), 175-193.

Houben, A. J., Bijl, P. K., Pross, J., Bohaty, S. M., Passchier, S., Stickley, C. E., ... & Expedition 318 Scientists. (2013). Reorganization of Southern Ocean plankton ecosystem at the onset of Antarctic glaciation. *Science*, *340*(6130), 341-344.

Kato, Y. (2020). Diatom-based reconstruction of the Subantarctic Front migrations during the late Miocene and Pliocene. *Marine Micropaleontology*, *160*, 101908.

Kim, J. H., Van der Meer, J., Schouten, S., Helmke, P., Willmott, V., Sangiorgi, F., ... & Damsté, J. S. S. (2010). New indices and calibrations derived from the distribution of crenarchaeal isoprenoid tetraether lipids: Implications for past sea surface temperature reconstructions. *Geochimica et Cosmochimica Acta*, *74*(16), 4639-4654.

Lenton, A., & Matear, R. J. (2007). Role of the southern annular mode (SAM) in Southern Ocean CO2 uptake. Global Biogeochemical Cycles, 21(2).

Marshall, J., & Speer, K. (2012). Closure of the meridional overturning circulation through Southern Ocean upwelling. *Nature Geoscience*, *5*(3), 171-180.

McClymont, E. L., Elmore, A. C., Kender, S., Leng, M. J., Greaves, M., & Elderfield, H. (2016). Pliocene-Pleistocene evolution of sea surface and intermediate water temperatures from the southwest Pacific. *Paleoceanography*, *31*(6), 895-913.

McKay, R., Naish, T., Carter, L., Riesselman, C., Dunbar, R., Sjunneskog, C., ... & Powell, R. D. (2012). Antarctic and Southern Ocean influences on Late Pliocene global cooling. *Proceedings of the National Academy of Sciences*, *109*(17), 6423-6428.

Meijers, A. J. S., Bindoff, N. L., & Rintoul, S. R. (2011). Frontal movements and property fluxes: Contributions to heat and freshwater trends in the Southern Ocean. *Journal of Geophysical Research: Oceans*, *116*(C8).

Mudie, P. J., Leroy, S. A. G., Marret, F., Gerasimenko, N. P., Kholeif, S. E. A., Sapelko, T., & Filipova-Marinova, M. (2011). Nonpollen palynomorphs: indicators of salinity and environmental change in the Caspian–Black Sea–Mediterranean corridor. *Geology and geoarchaeology of the Black Sea region: beyond the flood hypothesis*, *473*, 89-115.

Nooteboom, P. D., Bijl, P. K., van Sebille, E., Von Der Heydt, A. S., & Dijkstra, H. A. (2019). Transport bias by ocean currents in sedimentary microplankton assemblages: Implications for paleoceanographic reconstructions. *Paleoceanography and Paleoclimatology*, *34*(7), 1178-1194.

Orsi, A. H., Whitworth III, T., & Nowlin Jr, W. D. (1995). On the meridional extent and fronts of the Antarctic Circumpolar Current. *Deep Sea Research Part I: Oceanographic Research Papers*, *42*(5), 641-673.

Passchier, S. (2011). Linkages between East Antarctic Ice Sheet extent and Southern Ocean temperatures based on a Pliocene high-resolution record of ice-rafted debris off Prydz Bay, East Antarctica. *Paleoceanography*, *26*(4).

Prebble, J. G., Crouch, E. M., Carter, L., Cortese, G., Bostock, H., & Neil, H. (2013). An expanded modern dinoflagellate cyst dataset for the Southwest Pacific and Southern Hemisphere with environmental associations. *Marine Micropaleontology*, *101*, 33-48.

Raymo, M. E., Kozdon, R., Evans, D., Lisiecki, L., & Ford, H. L. (2018). The accuracy of mid-Pliocene δ18O-based ice volume and sea level reconstructions. *Earth-Science Reviews*, *177*, 291-302.

Rintoul, S. R., & Bullister, J. L. (1999). A late winter hydrographic section from Tasmania to Antarctica. *Deep Sea Research Part I: Oceanographic Research Papers*, *46*(8), 1417-1454.

Sangiorgi, F., Bijl, P. K., Passchier, S., Salzmann, U., Schouten, S., McKay, R., ... & Brinkhuis, H. (2018). Southern Ocean warming and Wilkes Land ice sheet retreat during the mid-Miocene. *Nature Communications*, *9*(1), 1-11.

Sluijs, A., Brinkhuis, H., Stickley, C. E., Warnaar, J., Williams, G. L., & Fuller, M. (2003). Dinoflagellate cysts from the Eocene/Oligocene transition in the Southern Ocean; results from ODP Leg 189. In *Proceedings of the Ocean Drilling Program. Scientific Results*.

Sluijs, A., Pross, J., & Brinkhuis, H. (2005). From greenhouse to icehouse; organic-walled dinoflagellate cysts as paleoenvironmental indicators in the Paleogene. *Earth-Science Reviews*, *68*(3-4), 281-315.

Sokolov, S., & Rintoul, S. R. (2009). Circumpolar structure and distribution of the Antarctic Circumpolar Current f ronts: 1. Mean circumpolar paths. *Journal of Geophysical Research: Oceans*, *114*(C11).

Stickley, C. E., Brinkhuis, H., McGonigal, K. L., Chaproniere, G. C. H., Fuller, M., Kelly, D. C., ... & Stant, S. A. (2004). Late Cretaceous–Quaternary biomagnetostratigraphy of ODP Sites 1168, 1170, 1171, and 1172, Tasmanian Gateway. In *Proceedings of the Ocean Drilling Program, Scientific Results* (Vol. 189, pp. 1-57). Ocean Drilling Program, College Station TX.

Stockhausen, M. (unpublished, M.Sc. thesis Utrecht University 2022). Latitudinal Subtropical Front Migration during the Early Piacenzian Stage of the Pliocene at the Agulhas Plateau, South Africa.

Tan, N., Ramstein, G., Dumas, C., Contoux, C., Ladant, J. B., Sepulchre, P., ... & De Schepper, S. (2017). Exploring the MIS M2 glaciation occurring during a warm and high atmospheric CO2 Pliocene background climate. *Earth and Planetary Science Letters*, *472*, 266-276.

Thoele, L.M., Nooteboom, P.D., Hou, S., Wang, R., Nie, S. Michel, E., … & Bijl, P. K. (unpublished). An expanded database of Southern Hemisphere surface sediment dinoflagellate cysts and their oceanographic affinities.

Whitehead, J. M., Quilty, P. G., Harwood, D. M., & McMinn, A. (2001). Early Pliocene paleoenvironment of the Sørsdal Formation, Vestfold Hills, based on diatom data. *Marine Micropaleontology*, *41*(3-4), 125-152.

Wrenn, J., Hannah, M. J., & Raine, J. I. (1998). Diversity and palaeoenvironmental significance of late Cenozoic marine palynomorphs from the CRP-1 Core, Ross Sea, Antarctica. *Terra Antartica*, *5*(3), 553-570.

Zonneveld, K. A., Marret, F., Versteegh, G. J., Bogus, K., Bonnet, S., Bouimetarhan, I., ... & Young, M. (2013). Atlas of modern dinoflagellate cyst distribution based on 2405 data points. *Review of Palaeobotany and Palynology*, *191*, 1-197.

Zonneveld, K. A., Versteegh, G., & Kodrans-Nsiah, M. (2008). Preservation and organic chemistry of Late Cenozoic organic-walled dinoflagellate cysts: A review. *Marine Micropaleontology*, *68*(1-2), 179-197.

8 Appendix

A Dinocyst taxa

Achomosphaera spp.
Ataxiodinium choane
Ataxiodinium confusom
Brigantedinium spp.
Cerebrocysta poulsenii
Echinidinium spp.
Echinidinium transparantum
Filisphaera
Habibacysta tectata
Impagidinium aculeatum
Impagidinium pallidum
Impagidinium paradoxum
Impagidinium patulum
Impagidinium sphaericum
Impagidinium velorum
Invertocysta tabulate
cf. Invertocysta tabulate
Islandinium spp.
Lingulolodinium macherophorum
Nematosphaeropsis labyrinthus
Operculodinium centrocarpum
Operculodinium eirikianum
Operculodinium israelinium
Operculodiniun janduchenii
Operculodinium sp. 1
Pentapharsodinium dalei
Polysphaeridium spp.
Pyxidinopsis reticulata
Selenopemphix quanta
Spiniferites bentorii
Spiniferites elongatus

Spiniferites membranaceus
Spiniferites mirabilis
Spiniferites ramosus
Spiniferites rubinus
Spiniferites splendidus
Spiniferites spp.
Tectatodinium psilatum
Tuberculodinium spp.

B Core photos

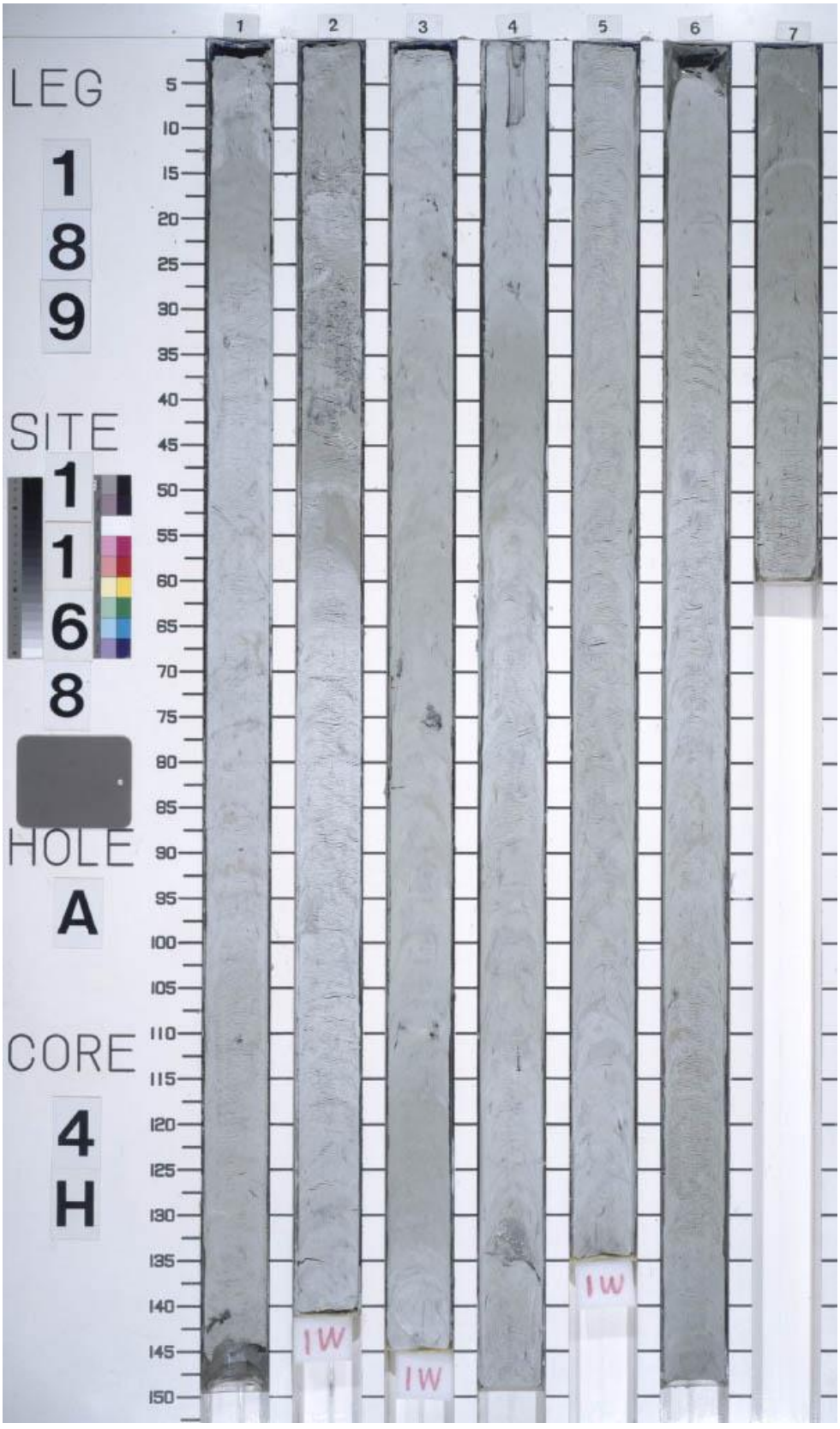

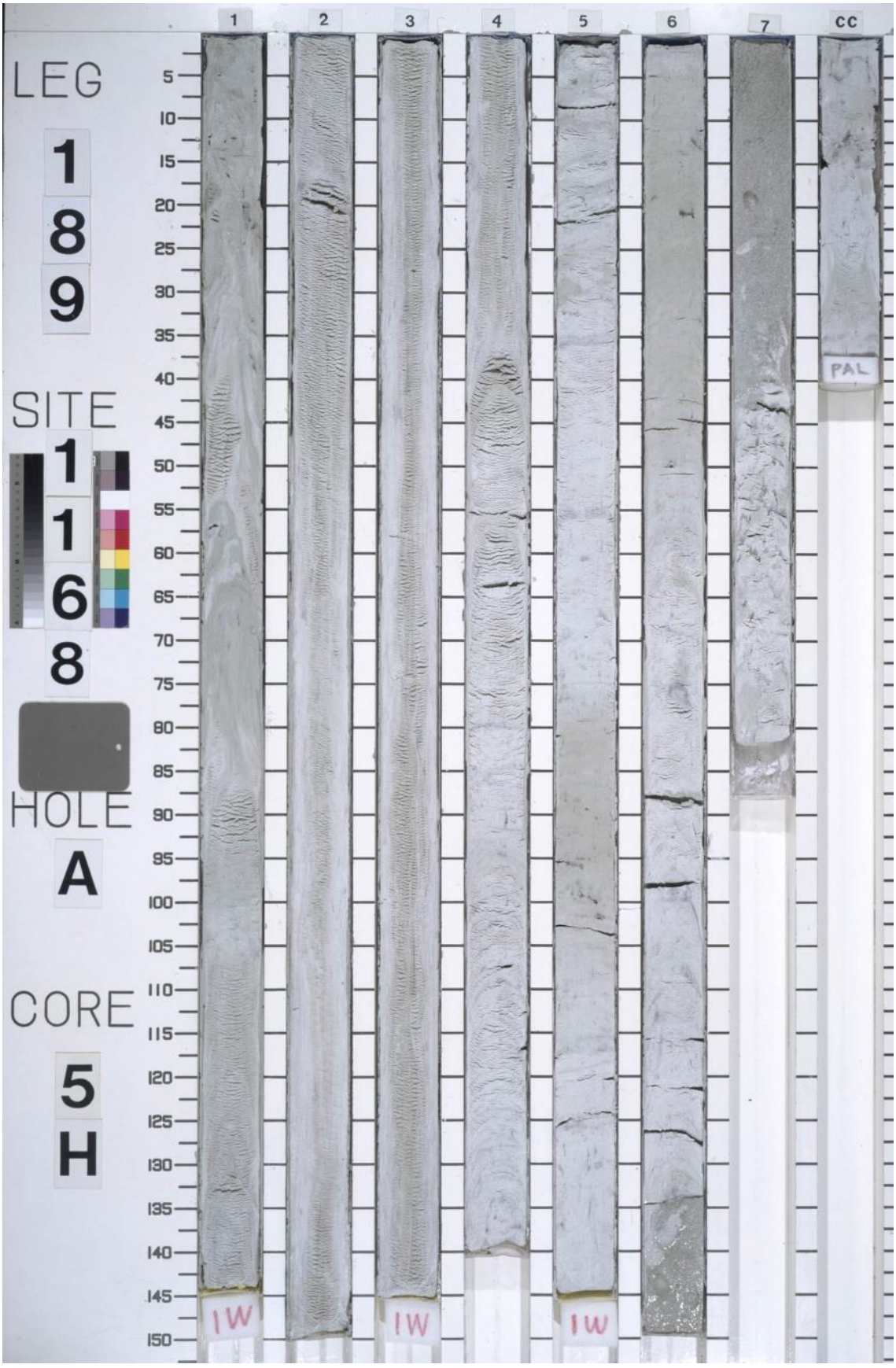
LEG
189
SITE
1168
HOLE
A
CORE
5
H
1
2
3
4
5
6
7
CC
PAL
IW
IW
IW

C Relative abundance of all dinocysts